BL-6A/2019G082

Deformation of "Single-Crystal-Like" Lamellar Structure Formed by a Liquid Crystalline Block Copolymer

Masatoshi TOKITA[1,*] and Ryohei ISHIGE[1]
[1] Department of Chemical Science and Engineering, Tokyo Institute of Technology, 2-12-1 Ookayama, Meguro, Tokyo 152-8550, Japan

1 Introduction

The response of a layered structure to external stresses has been extensively examined for ABA triblock copolymers composed of high glass transition temperature (T_g) A segments connected to both ends of a subzero T_g B segment because of their practical use of thermoplastic elastomers.[1–4] Such polystyrene-*block*-polybutadiene-*block*-polystyrene (SBS) copolymers form glassy/rubbery type lamellae of the polystyrene (PS)/polybutadiene (PB) segments at ambient temperatures. The direction of the force with respect to the lamellar normal affects the deformation mechanism, as confirmed when using single-crystal-like monodomain lamellar films prepared via the roll-casting method.[2,3] When force is applied perpendicular to the lamellae to increase the macroscopic strain, the lamellae tilt the normal away from the deformation direction and have sharp hinges to form chevron morphology. In contrast, when the temperature is raised to 100 °C to make the SBS form viscous/rubbery type lamellae of the PS/PB segments, the same deformation dilates the lamellae to increase the spacing without tilting them. Thus, the deformation mechanism of two-phase lamellae can be affected by the state of each lamella.

In this work, we investigate the deformation of viscous/LC lamellae composed of an LC block copolymer upon being stretched in a direction parallel to the lamellar normal. The LC block copolymer, herein designated as B5-*x*-EMA-φ, consists of a main-chain smectic LC BB-5(3-Me) polyester bonded at both ends to poly(ethyl methacrylate) (PEMA) segments (Fig 1).[5–9] *x* and φ is the number average molecular weight (M_n) of the BB-5(3-Me) segment and the PEMA segment volume percentage, respectively. The B5-*x*-EMA-φ copolymers at φ < 50 segregate these two types of segments from one another to form lamellar microdomains, within which the LC segment forms smectic layers lying parallel to the microdomain lamellae. A characteristic of B5-*x*-EMA-φ is the formation of fibers of a well-oriented "single-crystal-like" microstructure with the normal of both microdomain lamellae and smectic layers aligned along the fiber axis. Herein, we stretched the fibrous sample at a rate of 5% min^{-1}, and the sample stress and two-dimensional X-ray scattering were simultaneously measured. The X-ray scattering analysis discloses the deformation mechanism of the lamellar microdomain. With increasing the elongation ratio (λ) up to 1.6, the PEMA lamellae are preferentially dilated to cause the tilt of the lamellar normal with respect to the stretching direction, resulting in the lamellar undulation. With further increasing λ, the lamellae take chevron morphology that comprising straight parts connected with localized bends while recovering the spacing.

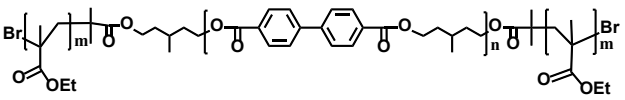

Fig. 1: Chemical structure of B5-*x*-EMA-φ

2 Experiment

The B5-26-EMA-41 was prepared according to the procedure reported previously.[5–9] The M_ns of the BB-5(3-Me) ($M_{n,LC}$) and PEMA ($M_{n,am}$) segments were 26,000 and 16,000, respectively, as determined via ^{1}H NMR spectroscopy. The polydispersity indices (PDIs) the LC segment and block copolymer were 1.89 and 1.60, respectively, as determined via size exclusion chromatography (SEC) with PS standards. The block copolymer exhibited a unimodal SEC peak. The DSC curve measured upon heating at a rate of 10 °C min^{-1} included a sharp increase in the heat capacity (36 °C) and an endothermic peak (154 °C), which were attributed to the glass transition and isotropization, respectively, of the smectic LC formed by the BB-5(3-Me) segment. The T_g of the PEMA measured for homo PEMA was 70 °C, although the T_g of the PEMA block was barely detected, likely due to the smaller PEMA fraction in the copolymer. At a temperature higher than the T_g, the PEMA block is viscous liquid rather than rubbery. The molecular weight of each PEMA segment at both ends ($M_{n,am}/2$ = 8,000) is comparable to the molecular weight of an entangled strand (M_e = 6,000) evaluated from rheological measurements.[10]

Synchrotron radiation small-angle X-ray scattering (SAXS) measurements were performed at the BL-6A beamline at the Photon Factory, Tsukuba, Japan, using a Dectris Pilatus 1M detector. The X-ray radiation wavelength (λ_X) was 0.15 nm. The sample-to-detector distance was 2 m. The fibrous sample at 80 °C was continuously stretched using a Linkam TST350 tensile stage at a crosshead speed of 1.2 μm s^{-1} (nominal strain rate 5% min^{-1}). The dimensions of the test samples were 0.60 × 0.021 × 1.5 mm. The X-ray scattering patterns were recorded at an exposure time of 30 s. The scattering intensity was presented as a function of the scattering vector $q = 4\pi \sin\theta/\lambda_X$, where 2θ was the scattering angle.

3 Results and Discussion

The stress (σ)–λ curve measured for B5-26-EMA41 is shown in Fig. 2. Upon increasing the λ, the sample exhibited a linear elastic response with Young's modulus of 7.5 MPa and a yield point at λ = 1.25. Then, the σ gradually decreased and showed a steeper decrease at 2.0 < λ < 2.3, where the sample might have rippled. The sample elongated up to λ = 3.3 had clacks. Thus, we examined the structural changes of B5-26-EMA41 stretched along the lamellar normal up to λ = 2.0.

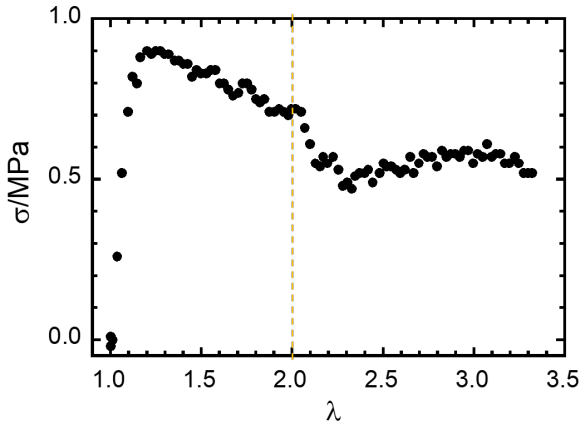

Fig. 2: The σ–λ curve measured at 80°C for a fibrous B5-26-EMA-41 sample with the normal of both the microdomain lamellae and smectic layers oriented parallel to the fiber axis.

Representative SAXS profiles measured simultaneously with the σ–λ curve are shown in Fig. 3 as a function of λ. At a small λ of 1.1, the SAXS patterns exhibited continuous shifting of the meridional peak position toward smaller values of the *q*. Upon increasing the λ over 1.2, the reflections spread in the azimuthal direction, suggesting undulation of the lamellae. Upon further increasing the λ to 1.7, the reflections split into quadrants to display a four-point pattern, which was attributed to a chevron structure consisting of predominantly straight layers but bent at localized hinge regions. The four-point reflections increased the splitting angle with the λ.

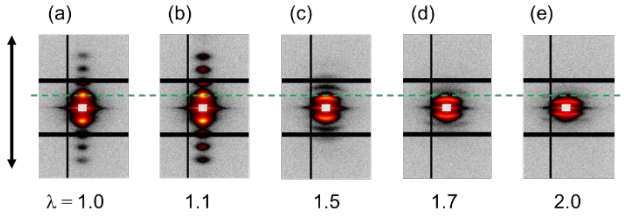

Fig. 3: SAXS patterns measured during deformation of a fibrous B5-26-EMA-41 sample at 80 °C, with the load applied parallel to the lamellar normal at the λ indicated below the pattern in each panel. The horizontal dotted line crossing all the panels indicates the first-order reflection position on the pattern measured at λ = 1.0 for ease of comparison of the reflection location.

To evaluate the changes in the lamellar spacing (*d*) with deformation, SAXS intensity profiles were obtained from the measured two-dimensional patterns by averaging the scattering intensity over azimuthal sectors of 10° on each side of the direction in which lamellar reflection intensity maxima were located (Fig. 4). The samples with λ < 1.6 displayed scattering maxima on the meridian, and each intensity curve included several maxima located at *q* with integer ratios. However, the samples with λ > 1.7 displayed scattering maxima in the quadrant, and each intensity curve included less than two maxima. The *d* estimated from the first-order scattering maximum was plotted as a function of λ in Fig. 5 with closed circles. It increased as the λ increased up to 1.6 before dropping and decreasing with further increases of λ.

In addition to the change in *d*, the deformation caused arcing or splitting of the lamellar reflection due to the folding of the lamellae. The samples at λ < 1.6 had undulated lamellae and displayed arced lamellar reflections. The average tilt angle of the lamellae with respect to the elongation direction, θ_{LAM}, was assumed to be equal to the half-width at half-maximum (HWHM) of the azimuthal scans of the first-order lamellar reflection.[3] The samples at λ > 1.7 had lamellae displaying four-point SAXS patterns ascribed to a chevron structure, with a θ_{LAM} equal to the azimuthal angle between the stretching direction (the meridional line) and the peak of the four-point pattern. The values of θ_{LAM} thus determined were plotted as a function of λ in Fig. 6 with triangles. Although the unstretched sample displayed a finite HWHM of 10°, possibly due to the fluctuations in the lamellar structure, the θ_{LAM} started increasing at λ = 1.2.

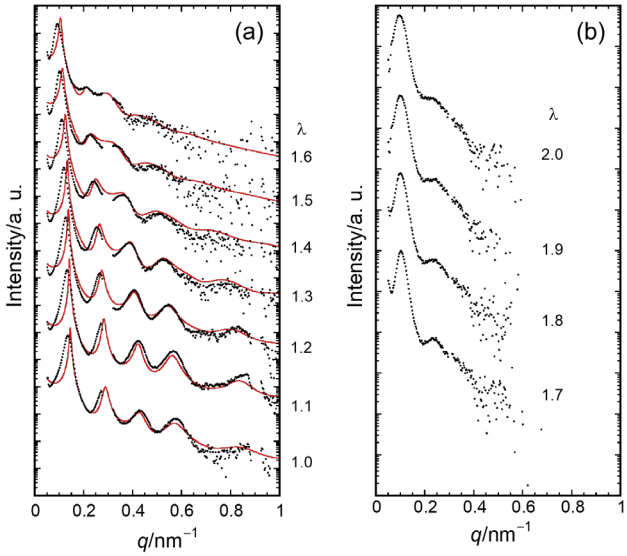

Fig. 4: SAXS intensity profiles measured for B5-26-EMA-41 fibers elongated at the λ indicated in the figure. The scattering intensity was obtained by averaging the scattering intensity profiles over azimuthal sectors of 10° on each side of (a) the meridian and (b) the direction along which the scattering maxima appeared to show a four-point pattern. The solid curves in (a) indicate the calculated intensity on the basis of the ideal two-phase lamellar model.

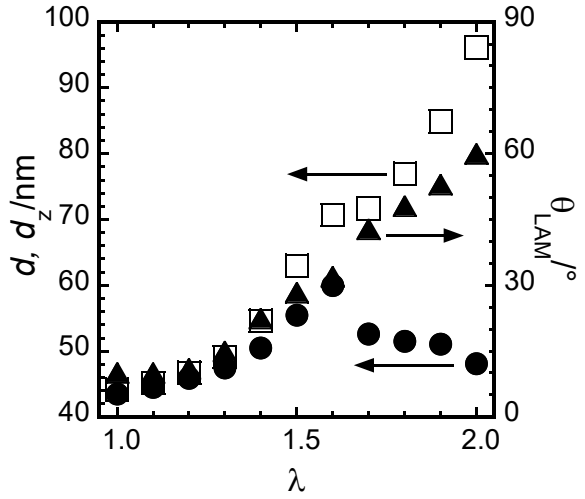

Fig. 5: Changes in the spacing, d (circles), and tilt angle, θ_{LAM} (triangles), with respect to the fiber axis as a function of λ during the elongation of a fibrous B5-26-EMA-41 fiber at 80 °C. The repeat length of stacked lamellae along the fiber axis, d_z, was calculated from the equation $d_z = d/\cos\theta_{LAM}$, and the values were plotted with squares.

The effects of sample deformation on the lamellar structure seemed to differ depending on the λ. The sample deformation at $\lambda < 1.6$ preferred to increase d rather than to tilt the lamellae, whereas that at $\lambda > 1.6$ preferred to rotate the lamellae about an axis perpendicular to the stress direction rather than dilate them. As shown in Fig. 6, the d increased with the λ in the range of $\lambda < 1.6$ and tended to recover upon further deformation, while the θ_{LAM} continuously increased with the λ. Meanwhile, such a change of the lamellar deformation mechanism did not affect the σ–λ curve, and the σ monotonically decreased as the λ increased from 1.25 to 2.0, passing the λ at which the deformation mechanism changed (see Fig. 2).

This LC block copolymer deformation preferentially dilated the PEMA block lamellae. The LC and PEMA block lamellar thicknesses were evaluated by comparing the scattering intensity observed with that calculated on the basis of the ideal two-phase model,[11] as shown by solid line curves in Fig. 4a. In Fig. 6, the ratio of the lamellar thickness in a stretched sample to that of an unstretched sample was plotted against the λ for the LC block lamellae ($d_{LC}/d_{LC,0}$) and the PEMA block lamellae ($d_{am}/d_{am,0}$). The ratio of the lamellar spacing (d/d_0) was also plotted in the same figure. Comparing the ratio between them at the same $\lambda = 1.60$, $d_{am}/d_{am,0} = 1.51$ was greater than $d_{LC}/d_{LC,0} = 1.29$, and d/d_0 took an intermediate value of 1.38. Such a small deformation of the LC block lamellae could be explained by the fact that this deformation involved an energetically costly smectic layer undulation, although the LC segment had a lower T_g than the PEMA segment.

The preferential dilation of the PEMA segment lamellae was associated with the tilt of the lamellar microdomains. In the dilated lamellae, PEMA segments were more elongated along the lamellar normal than LC segments to occupy a smaller area on the lamellar interface than the connecting LC segments. Assuming that this interfacial area difference between these two segments was compensated by tilting the interface normally with respect to the fiber axis, the θ_{LAM} was equal to $\cos^{-1}[(d_{LC}/d_{LC,0})/(d_{am}/d_{am,0})]^{0.5}$. In Fig. 6b, the calculated value of $\theta_{LAM,calc}$ was plotted against the $\theta_{LAM,obs}$ measured via SAXS. Although the plots at a smaller λ showed discrepancies from the expected line due to errors stemming from fluctuations in the deformed lamellar structure and the estimation of $\theta_{LAM,obs}$, the $\theta_{LAM,calc}$ agreed well with the $\theta_{LAM,obs}$. This let us ascribe the tilting of the lamellae to the preferential dilation of the PEMA block lamellae upon the elongation.

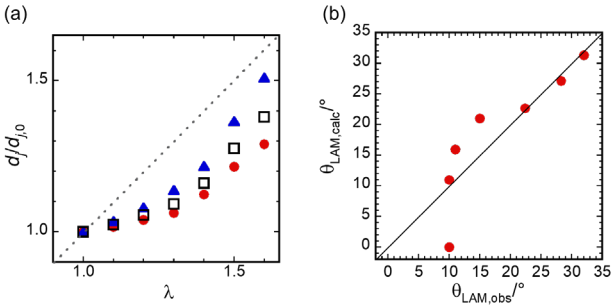

Fig. 6: (a) Dilation of LC block lamellar thickness, $d_{LC}/d_{LC,0}$ (circles); PEMA block lamellar thickness, $d_{am}/d_{am,0}$ (triangles); and lamellar spacing, d/d_0 (open squares), in the state stretched at λ. (b) Plots of the lamellar tilt angle, $\theta_{LAM,calc}$, calculated assuming the preference dilation of PEMA block lamellae against the $\theta_{LAM,obs}$ measured via SAXS.

Acknowledgement

4,4′-dimethyl biphenyldicarboxylate was kindly supplied by Iharanikkei Chemical Industry Co. Ltd. This work was supported by JSPS KAKENHI for Scientific Research on Innovative Areas “MFS Materials Science (Grant Number JP19H05120)”, and JSPS KAKENHI Grant Number JP19H02770.

References

[1] M. Fujimura et al., *Rubber Chem. Technol.* **51**, 215 (1978).
[2] Y. Cohen et al., *Macromolecules* **33**, 6502 (2000).
[3] Y. Cohen et al., *J. Chem. Phys.* **114**, 984 (2001).
[4] S. Hölzer et al., *Eur. Polym. J.* **49**, 261 (2013).
[5] R. Ishige et al., *Macromolecules* **44**, 4586 (2011).
[6] M. Koga et al., *Macromolecules* **45**, 9383 (n.d.).
[7] M. Koga et al., *Macromol. Chem. Phys.* **214**, 2295 (2013).
[8] M. Koga et al., *Macromolecules* **47**, 4438 (2014).
[9] M. Hayashi et al., *Polymer* **178**, 121555 (2019).
[10] J. Hrouz et al., *Die Makromol. Chemie* **181**, 277 (1980).
[11] R.-J. Roe, *Methods of X-Ray and Neutron Scattering in Polymer Science* (Oxford University Press, 2000).

* tokita.m.aa@m.titech.ac.jp